Computational Materials Science 46 (2009) 383–392

Contents lists available at ScienceDirect

Computational Materials Science

journal homepage: www.elsevier.com/locate/commatsci

Virtual material testing for stamping simulations based on polycrystal plasticity

M. Kraska [a,*], M. Doig [a], D. Tikhomirov [a], D. Raabe [b], F. Roters [b]

[a] INPRO Innovationsgesellschaft für fortgeschrittene, Produktionssysteme in der Fahrzeugindustrie, Hallerstraße 1, 10587 Berlin, Germany
[b] Max-Planck-Institut für Eisenforschung, Max-Planck-Straße 1, 40237 Düsseldorf, Germany

ARTICLE INFO

Article history:
Received 5 March 2009
Accepted 13 March 2009
Available online 21 April 2009

PACS:
07.05.Tp
46.15.−x
61.66.Bi
81.40.Lm
81.70.−q

Keywords:
Virtual material testing
Stamping simulation
Texture
Crystal plasticity finite element method

ABSTRACT

In the modern practice of stamping simulation of complex industrial parts the prediction of springback still lacks accuracy. In commercial software packages various empirical constitutive laws for stamping are available. Limited to simple empirical models for material anisotropy they do not take into account in a full manner the effects of microstructure and its evolution during the deformation process. The crystal plasticity finite element method bridges the gap between the polycrystalline texture and macroscopic mechanical properties that opens the way for more profound consideration of metal anisotropy in the stamping process simulation. In this paper the application of crystal plasticity FEM within the concept of virtual material testing with a representative volume element (RVE) is demonstrated. Using virtual tests it becomes possible, for example, to determine the actual shape of the yield locus and Lankford parameters and to use this information to calibrate empirical constitutive models. Along with standard uniaxial tensile tests other strain paths can be investigated like biaxial tensile, compressive or shear tests. The application of the crystal plasticity FEM for the virtual testing is demonstrated for DC04 and H320LA steel grades. The parameters of the Vegter yield locus are calibrated and the use case demonstration is completed by simulation of a typical industrial part in PAMSTAMP 2G.

1. Introduction

The highly competitive automotive market demands for lightweight and safe vehicles. These requirements can be met using, for example, high strength multiphase steels. Along with the positive service properties like higher strength and energy absorption during crash these steels tend to higher springback after forming. The modern forming technology is aimed at early compensation of springback by corresponding modification of the tool geometry Roll et al. [20]. In order to comply with shape tolerances, iterative tool modifications are required. Reliable simulation tools with exact springback prediction are required which can considerably accelerate the stamping tool design and optimization process and reduce the time before the start of production.

Various factors have a significant impact on springback simulation results. Tool shape (drawing radii), discretization (mesh density, element types), contact and friction between sheet and stamping tool as well as the elastoplastic sheet material behavior during the process influence the resulting springback. In this paper we restrict our attention to the latter aspect, namely material modeling. The demands of industrial applicability of springback simulation comprise reliable stress prediction, handling of multiaxial loads and load direction change, accounting for sheet orthotropy as well as isotropic and kinematic hardening phenomena (Bauschinger effect).

Commercial software packages offer a variety of empirical constitutive laws for stamping simulations, a comprehensive overview of these models can be found in Banabic et al. [4]. In the most cases the constitutive laws by Hill [9,10] and Barlat (Barlat et al. [5], Barlat and Lian [6]) are used for stamping simulations. The evolution of material properties is usually modeled by isotropic and/or kinematic hardening with linear (Prager [18] type) or nonlinear (Ziegler [24] or Armstrong and Frederick [1] type) evolution of back stress. The empirical laws are well suited for industrial stamping simulation, particularly because of relatively short computation times and the macroscopic character of the most model parameters which normally can be identified from standard testing procedures.

However, sometimes, as practice shows, a reliable prediction of springback after die opening cannot be achieved. One of the drawbacks of the most empirical formulations is the insufficient consideration of changing material anisotropy due to microstructure evolution. In this sense, microstructural models can help to better identify the macroscopic properties of the empirical model. Microstructural models based on texture allow the user to include more physics associated with crystalline anisotropy, although they lead to longer computation times. In this article we pay attention to

* Corresponding author.
E-mail address: martin.kraska@inpro.de (M. Kraska).

0927-0256/$ - see front matter © 2009 Elsevier B.V. All rights reserved.
doi:10.1016/j.commatsci.2009.03.025

the crystallographic anisotropy of polycrystalline materials rather than morphological microstructure anisotropy. The physical background of crystallographic anisotropy is the crystalline arrangement of atoms. Each grain of the metallic material has a different crystallographic orientation, shape and volume fraction. The discrete nature of crystallographic slip along densely packed lattice directions on preferred slip planes also contributes to the overall anisotropic response of material. Moreover, individual crystals rotate and interact during forming. This leads to strong heterogeneity of strains and stresses. Texture and anisotropy gradually change, even under constant strain path condition. The presented approach demonstrates the use of performing of various virtual tests on a representative volume element (RVE) using the crystal plasticity model to identify the macroscopic yield behavior of the material and to extract hereof parameters for industrial stamping simulations.

The goal of this article is to present a virtual technique to determine the material parameters characterizing the ductile metal behavior (yield locus and *r*-values). It enables to considerably reduce the experimental expenses. That is of particular importance for the industrial goals, because in this way both cost and time savings can be achieved. The presented model is more complex than a conventional Taylor model but is limited in order to get the plausible results in a limited time. In this model the simplest approximation of a grain via one finite element is used. In this case the grain morphology is not taken in account, however, this is the easiest way to keep the model complexity within certain bounds. Extensions of this model to mutually opposed limit states – discretisation of a single grain with many finite elements or assuming many grains (orientations) in each integration point – are possible but the experimental and numerical complexity to adjust the model will grow.

The influence of the discretization on strength and stiffness of the aggregate has been investigated previously in Kraska [12]. The influence of the number of elements per grain has been separated from the stiffening influence of different boundary conditions (periodic boundary conditions versus suppressed local fluctuations at the RVE boundary). It was found that for moderate numbers of elements per grain, convergence cannot be expected (up to 320 constant strain elements per grain have been considered, this corresponds to $4 \times 4 \times 4$ cubes per grain). Thus, the choice of the discretization level is always a trade-off between good texture representation (number of grains) and good representation of local strain fluctuations (non-homogeneities, requiring fine meshes on grain level). Obviously, a pragmatic choice has to be made based on the acceptable computational costs. This choice has to be kept from the initial slip system calibration based on tensile tests throughout all virtual testing. Different levels of grain discretization provide different slip system calibrations. However, as long as the aggregate is able to represent the main features of the deformation induced texture, reasonable extrapolation can be expected. Even with coarse discretization, the model is still superior to simple mixing rules (Taylor model); because the induced textures are more realistic and local strain fluctuations are still allowed for.

This paper is organized as follows. After a brief overview of the technique of the crystal plasticity FEM the concept of virtual material testing using representative volume element is described.

Virtual tests enable to replace the costly numerous uniaxial tensile experiments and give the opportunity to investigate those stress and strain states which are not a standard in the material testing practice like biaxial tensile, compressive or shear tests.

The application of the crystal plasticity FEM for the virtual testing is demonstrated for DC04 and H320LA steels. The ability of the model to simulate the rolling texture of steel is shown. The effects of different boundary conditions of RVE and element types on the nominal stresses and Lankford parameters are numerically investigated. The pronounced Bauschinger effect for texture-based RVE is demonstrated by cyclic uniaxial tests. As a potential application a complex part has been simulated using the Vegter yield locus in PAMSTAMP 2G. This model interpolates over many tests, which in the present case have been run virtually. The perspectives and limitations of the applied approach are discussed.

2. Crystal plasticity finite element method

The crystal plasticity FEM (Pierce et al. [16,17], Asaro [2], Asaro and Needleman [3]) combines the basic process of crystallographic slip with the finite element method. Assume that the plastic velocity gradient $\mathbf{L}^p$ is composed out of the shear contributions $\dot{\gamma}^\alpha$ of all slip systems α:

$$\mathbf{L}^{\mathrm{p}} = \sum_{\alpha=1}^{n} \dot{\gamma}^\alpha \mathbf{S}^\alpha \tag{1}$$

where $\mathbf{S}^\alpha$ is the Schmid matrix of slip system α defined as $\mathbf{S}^\alpha = \mathbf{m}^\alpha \otimes \mathbf{n}^\alpha$ where $\mathbf{m}^\alpha$ is the slip direction and $\mathbf{n}^\alpha$ the slip plane normal. $\mathbf{L}^p$ is integrated to $\mathbf{F}^p$, plastic part of the multiplicative decomposition of the deformation gradient $\mathbf{F}$

$$\mathbf{F} = \mathbf{F}^{\mathrm{e}}\mathbf{F}^{\mathrm{p}} \tag{2}$$

using the flow rule

$$\dot{\mathbf{F}}^{\mathrm{p}} = \mathbf{L}^{\mathrm{p}}\mathbf{F}^{\mathrm{p}} \tag{3}$$

The crystal plasticity concept is implemented into the commercial FEM software MSC.Marc200x and ABAQUS/Standard by means of user subroutines. The implementation follows the scheme given by Kalidindi et al. [11]. The plastic shearing rates $\dot{\gamma}^\alpha$ on the slip systems α are taken as

$$\dot{\gamma}^\alpha = \dot{\gamma}^0 \left| \frac{\tau^\alpha}{\tau^\alpha_{\mathrm{crit}}} \right|^{\frac{1}{m}} \mathrm{sgn}(\tau^\alpha) \tag{4}$$

where τ^α is the resolved shear stress for the slip system α, and $\tau^\alpha_{\mathrm{crit}}$ is the current critical shear stress of slip system α. $\dot{\gamma}^0$ and m are material parameters representing reference shearing rate and the rate sensitivity of slip. The evolution of $\tau^\alpha_{\mathrm{crit}}$ is calculated including latent hardening through the following set of equations:

$$\dot{\tau}^\alpha_{\mathrm{crit}} = \sum_\beta h^{\alpha\beta} |\dot{\gamma}^\beta|; \quad h^{\alpha\beta} = q^{\alpha\beta} h^\beta; \quad h^\beta = h_0 \left(1 - \frac{\tau^\beta_{\mathrm{crit}}}{\tau_s} \right)^a \tag{5}$$

where $h^{\alpha\beta}$ is the rate of strain hardening on slip system α due to a shearing on slip system β, $q^{\alpha\beta}$ is the hardening matrix describing the latent hardening behavior of a crystallite, h^β is the hardening rate of the single slip system β, h_0 is the initial hardening, τ_s the saturation stress of the slip systems and a a hardening parameter.

2.1. The texture component CP-FEM

The recently introduced texture component crystal plasticity finite element method (TCCP-FEM) (Zhao et al. [23], Raabe and Roters [19]) is basically a combination of crystal plasticity FEM with the texture component method for the representation of statistical textures. The basic idea of the texture component method is the approximation of X-ray textures in the form of the orientation distribution function (ODF) by a discrete set of simple distribution functions (texture components) defined in orientation space. It was developed by Lücke et al. [14,13] and later on facilitated and implemented into an easy to use computer program[1] by Helming [7], [8, see also].

[1] The software "Multex 1.0" can be downloaded from http://www.texture.de.

The mathematical reproduction of the orientation distribution function $f(g)$ by texture component functions can be expressed by the superposition

$$f(g) = F + \sum_{c=1}^{C} I^c f^c(g) = \sum_{c=0}^{C} I^c f^c(g) \quad \text{where} \quad I^0 = F, \quad f^0(g) = 1 \tag{6}$$

where g is the crystallographic orientation and F is the volume portion of all randomly oriented crystals (random texture component). F may be understood as the intensity of the only global component used in the approximation, equivalent to $f^c(g) = 1$ for each orientation point in Euler space, $g \in G$. The intensity I^c describes the volume fraction of all crystallites belonging to the component c. $f^c(g)$ describes the orientation density of the component. For details about the implementation we refer to Zhao et al. [23], Raabe and Roters [19].

3. Virtual specimen (RVE)

Currently the direct use of crystallographic slip models for industrial forming simulations is not realistic, due to high computational costs. However, the complex models which incorporate microstructural information like slip systems and orientation distribution (Fig. 1) have the potential for extrapolation from simple calibration tests to arbitrary strain histories. Therefore, it is straightforward to use such models as virtual specimens. We call the process of running virtual tests for the identification of empirical models virtual material testing. When the virtual specimen is sufficiently reliable strain paths can be tested which in reality would be very expensive or even impossible to perform.

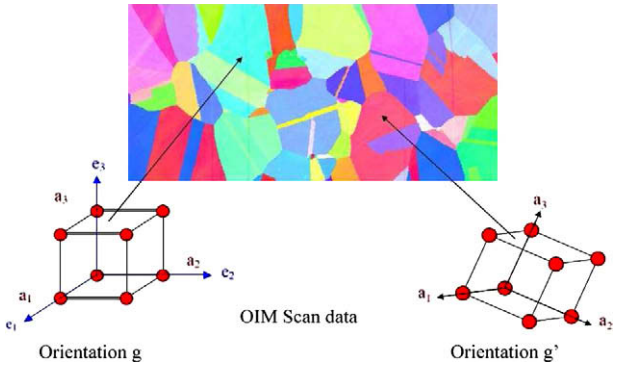

Fig. 1. Microscopic orientation image of a metallic sample. Each grain consists of uniformly oriented single crystals.

3.1. Model assumptions

The virtual specimen is a geometrical model of a representative volume element of real material. It is based on the crystal plasticity finite element method developed by MPIE (Zhao et al. [23], Raabe and Roters [19]). The most important model assumptions for the virtual specimen realized by INPRO are:

- The material consists of many differently oriented grains, each of them is represented by a single element. In succeding developments cubic body centered materials (ferritic steels DC04, H320LA) will be considered. The model can also be applied to face centered materials (austenitic steels, aluminum, copper).
- Single crystal grains possess both elastic and plastic anisotropy. The corresponding elastic values are taken from Teodosiu [21].
- Grains undergo plastic deformation due to displacement of neighbouring atom layers (slip planes) along preferred slip directions, in each crystal 48 slip systems for bcc and 12 for fcc grids are used. The displacements due to slip of grain interfaces, twinning and phase transformations are not currently covered by the model.
- Slip systems are considered active if the critical shear stress is exceeded. This critical shear stress corresponds to the yield curve of empirical model. The behavior of each slip system is described by viscous flow rule and incremental hardening law, see Kalidindi et al. [11].
- As the parameters are to be determined from simple tensile tests the hardening coefficient of all 48 bcc slip system classes are assumed to be identical. This is close to the pencil glide model, where the slip direction is restricted to the $\langle 1\,1\,1 \rangle$ class and the slip planes are those with the highest resolved shear stress.
- The strain history specified by the velocity gradient $\mathbf{L}(t)$ is applied such that the boundaries of the RVE are periodic. The stress response is calculated from the reaction force in the control nodes for the periodic boundary MPCs (multipoint constraints). The choice of periodic boundary conditions is motivated in Section 3.3.

Fig. 2 illustrates the virtual sample used in the present work, consisting of 1000 differently oriented grains represented by one volume element, respectively. From prescribed velocity gradient the deformation gradient is computed. Due to different grain orientations deformations of single crystals are different, the same is valid for stresses. Via homogenisation procedure the total nominal stress tensor in the form of the first Piola–Kirchhoff stress tensor is determined.

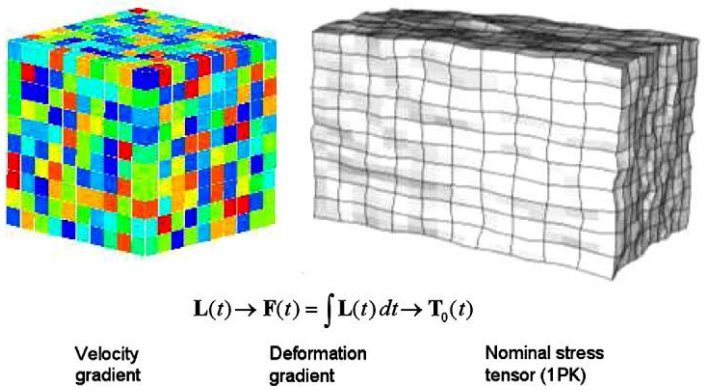

Fig. 2. Discretisation and strain control of the virtual sample.

3.2. Orientation distribution

The initial orientations of the grains in the RVE follow from random sampling of the texture components as obtained from pole figures (Figs. 3 and 4) using Multex program.

Texture development is an important cause for deformation induced anisotropy. The ability of the virtual specimen to predict deformation textures is demonstrated for the cold rolling process (Fig. 5).

Starting from a uniform orientation distribution the thickness of the specimen is reduced while the width remains constant. The simulated and measured pole figures look very similar even though small quantitative differences exist (Fig. 5). Possibly, if the cold rolling degree is known, texture measurement is no longer necessary because the texture can be obtained from the rolling simulation

3.3. Boundary conditions

Dependent of the superimposed averaged deformation, the following variants are considered (see Fig. 6)

- Homogeneous deformation. All nodes are moved so that the local deformation field is uniform. The grains are not in equilibrium. This corresponds to the Taylor model.

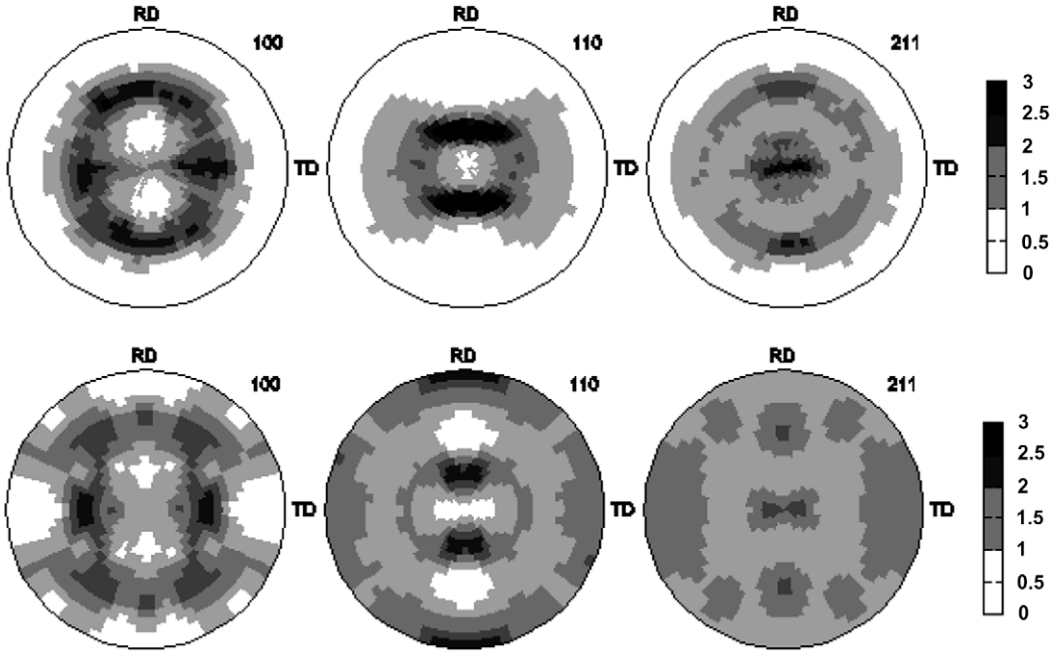

Fig. 3. Measured and recalculated pole figures, DC04.

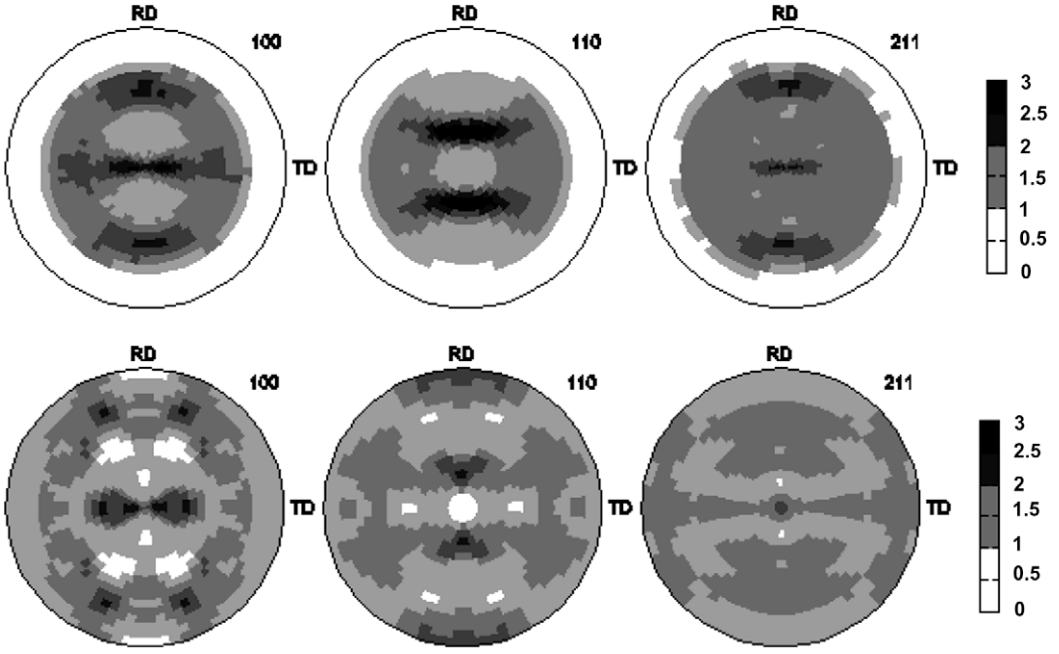

Fig. 4. Measured and recalculated pole figures, H320LA.

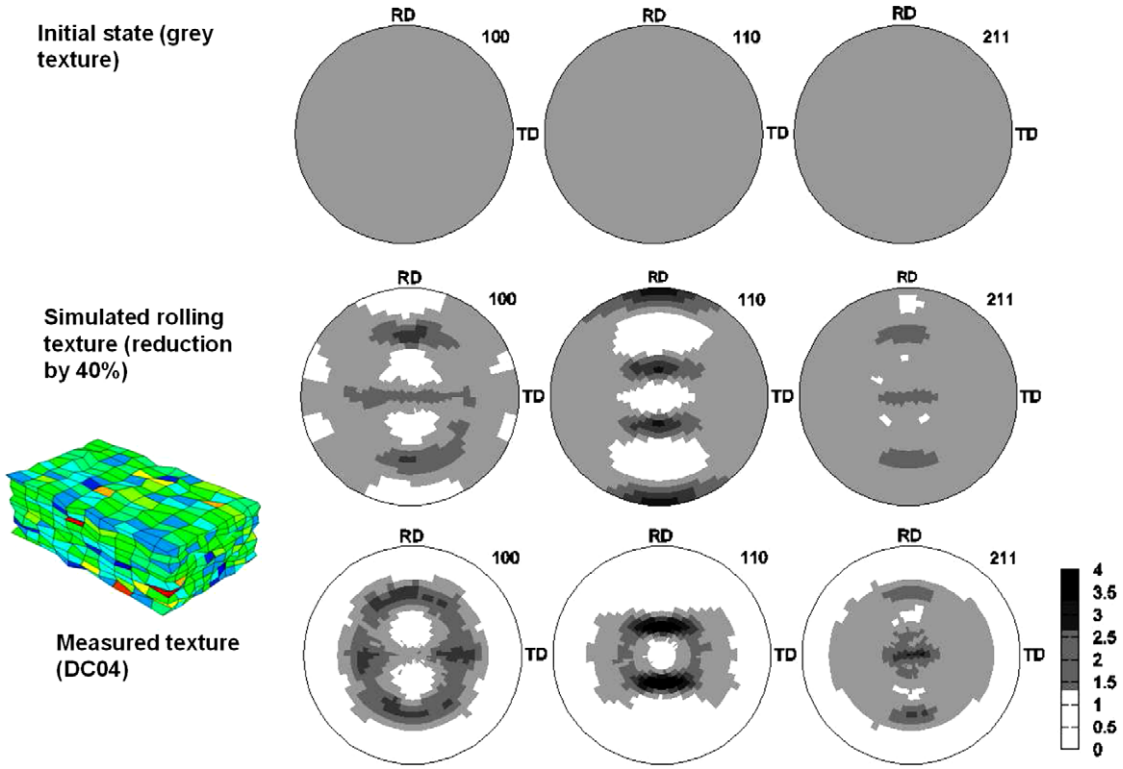

Fig. 5. Comparison between measured and simulated rolling texture.

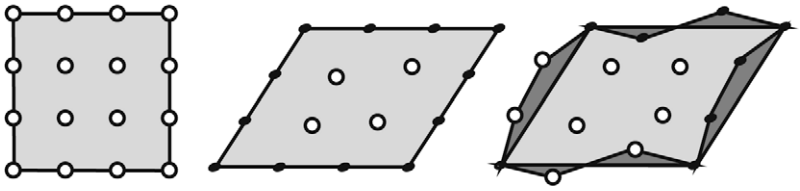

Fig. 6. Finite element nodes in reference state (left) and deformed with homogeneous boundary deflection (center) and periodic boundary deflection (right) as in Kraska [12].

- Homogeneous boundary. At the boundary, the nodal displacement is prescribed by the global strain. Inside the model, non-homogeneous deformations are possible. The internal nodes are in equilibrium while the boundary nodes generally are not.
- Periodic boundary. All nodal displacements are free but the model has to be periodic at the three space directions. This implies an indirect restriction to the boundary nodes. However, these are in equilibrium with their counterparts at opposite sides.

In Fig. 7 the deformation of the virtual specimen by different boundary conditions is shown. All of these constraints allow the exact prescription of the overall deformation. The periodic boundary conditions imply the least severe restrictions to prevent local non-homogeneous deformation of differently oriented grains. Correspondingly, the stress level for this type of boundary conditions (Fig. 8) is lowest. The *r*-value also shown in Fig. 8 is defined for tensile specimens as the ratio of the logarithmic strain in the width direction to the logarithmic strain in the thickness direction. Herewith the *r*-value is technologically important parameter in the stamping simulation that characterizes the sheet resistance against thickness reduction. Peridodic boundary conditions are used throughout the article because they imply the least artificial restrictions to the displacement field.

3.4. Influence of element type

Not only the boundary conditions, but also the type of element constrains the local motion posibilities of the virtual specimen. Tests for four different element types (linear and quadratic, reduced and fully integrated) were performed. The RVE with eight nodes and reduced integration elements (C3D8R) shows the highest displacement fluctuations (Fig. 9). This partly could be due to the hourglassing effect. The hourglass stiffness was calibrated to meet the C3D20R yield curve. Quadratic elements reproduce inhomogeneous deformation more accurately. The fully integrated elements lead to a higher tensile strength than the reduced ones (Fig. 9). The reduction in CPU time and the small differences in the calculated tensile strength justify the use of C3D8R elements for the planned tests.

3.5. Calibration and verification

The virtual specimen is calibrated (determination of the hardening parameters in slip system) on the basis of uniaxial tensile tests in the rolling direction (0). This leads to the hardening parameters given in Fig. 10 The quality of the model prediction is evaluated by comparing corresponding simulations to the remaining experimental data (stress–strain response and *r*-value of tensile tests in different directions and tension–compression tests). The

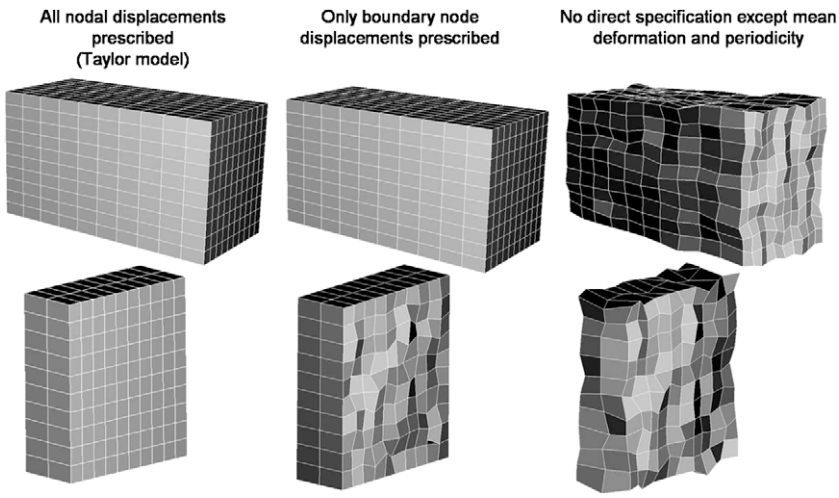

Fig. 7. RVE with different boundary conditions, DC04.

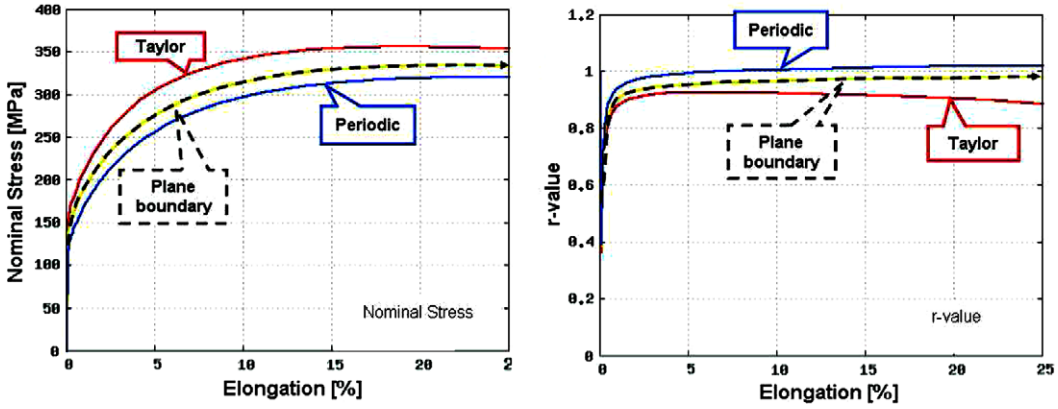

Fig. 8. Stress–strain response and *r*-value for different boundary conditions, DC04.

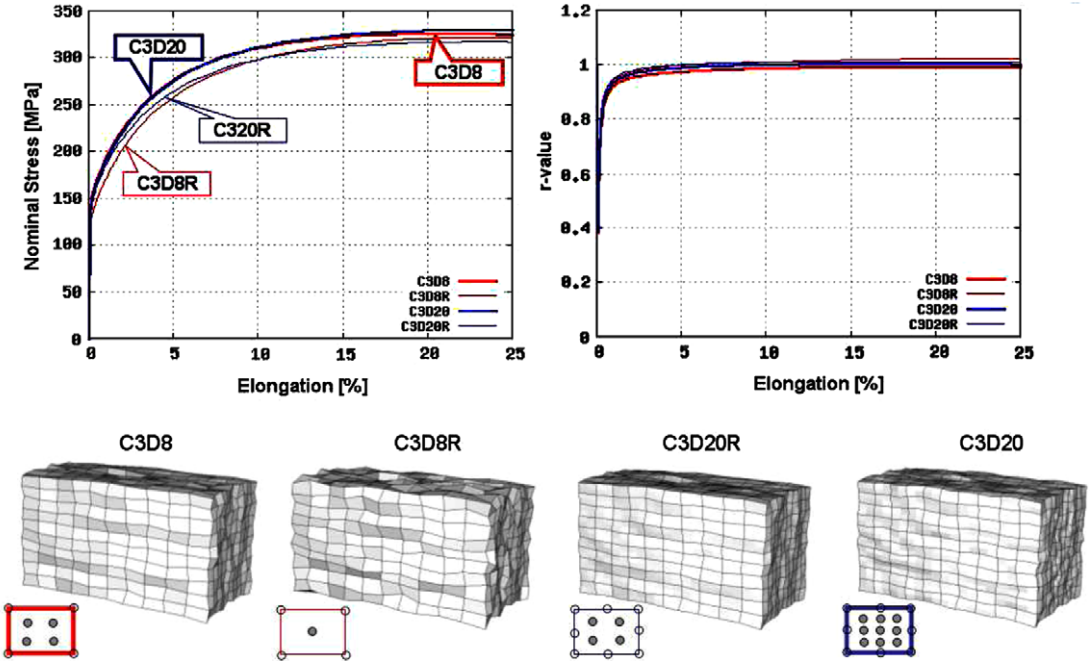

Fig. 9. Stress–strain response and *r*-values for different element types.

Parameter	DC04	H320LA
h_0	1293.	5569.
τ_s	48.	101.
a	7.	3.5

Fig. 10. Hardening parameters from the calibration of the virtual specimen.

stress–strain response for tensile tests under 45° and 90° is well predicted (Fig. 11). Only the tensile stress under 45° for DC04 is slightly underestimated (Fig. 11c). The estimated error is below 1.6%. The prediction for *r*-values are poor. In particular, for the cold rolling steel DC04 the simulated values for 0° and 45° are very low (Fig. 12). For the steel H320LA the situation is somewhat better as can be seen in Fig. 12.

3.6. Bauschinger effect

The ability of the model to predict the Bauschinger effect is evaluated comparing with tension–compression data. In order to compare the measurements with the simulation, two different curve representations are chosen. The direct comparison is obtained from the stress–strain curves. Fig. 13 shows that the simulated results for 0° agree with the measured curve, also after stress reversal from tension into compression. Even smooth transition to reversal of plastic flow is reproduced quite well. The Bauschinger effect (lower equivalent stress after change of loading direction) can also be illustrated by plotting the equivalent stress against the plastic equivalent strain (Fig. 14). In contrast to results from the virtual specimen, the measured curve shows a softening effect during high compression strain ranges (equivalent stress drop down). This can be traced back to instability of the specimen (buckling). In phenomenological (empirical) material models the Bauschinger effect is described using kinematic hardening. The virtual specimen does not include any explicit kinematic hardening. The reproduction of this effect is exclusively due to internal stresses between the grains.

4. Examples

It is very time and cost intensive to simulate a stamping process with crystal plasticity. Therefore, empirical material models are used in stamping simulation software. To obtain the right (empir-

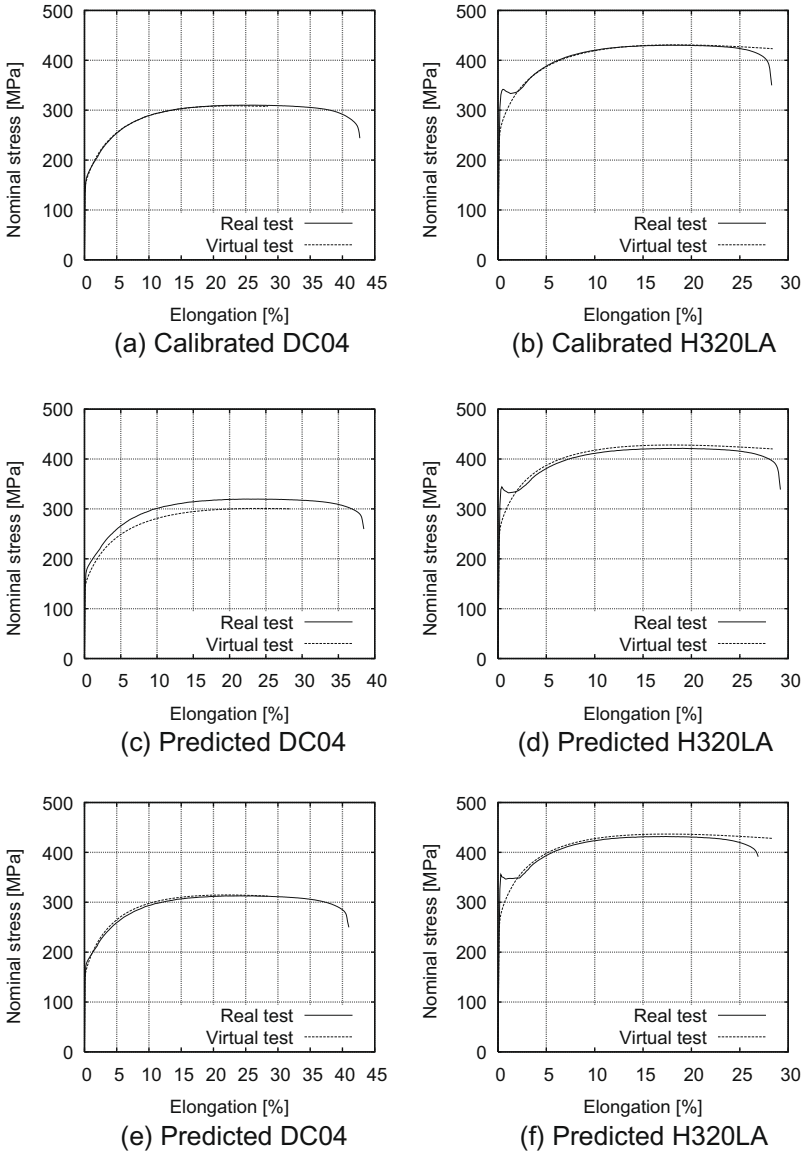

Fig. 11. Stress–strain response. Calibration and prediction. (a and b) Tensile test 0°; (c and d) tensile test 45°; (e and f) tensile test 90°.

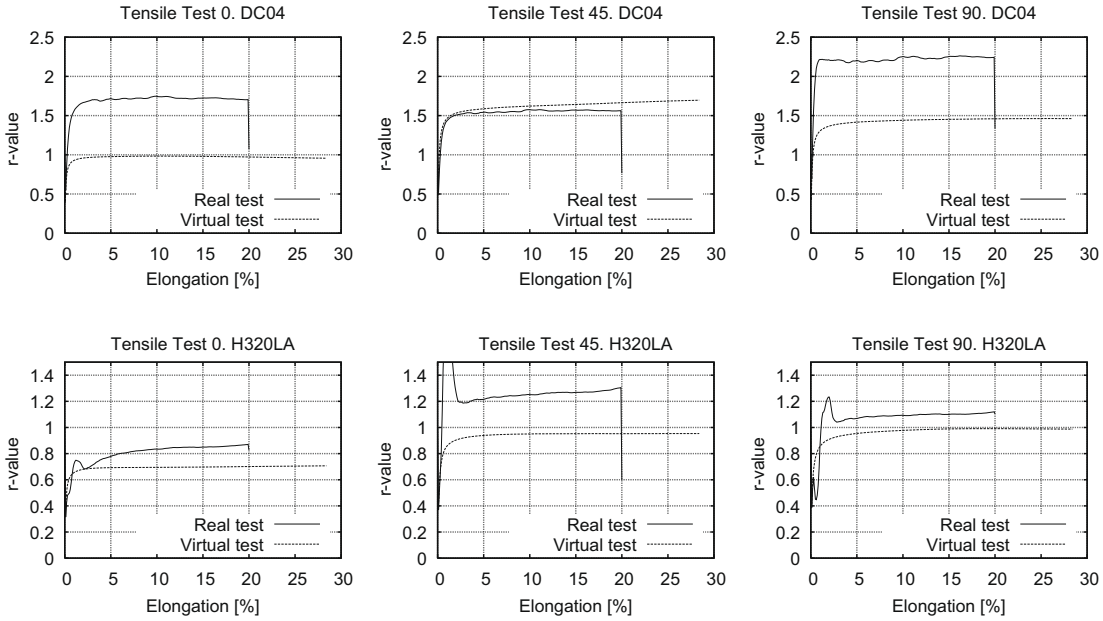

Fig. 12. r-Values for simulated tensile tests 0°, 45° and 90°.

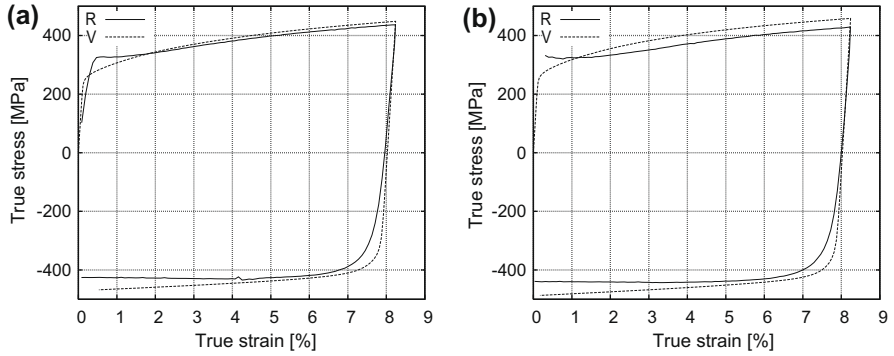

Fig. 13. Comparison between measured (R) and predicted (V) stress–strain curves of tension–compression tests in (a) 0° and (b) 90°, H320LA.

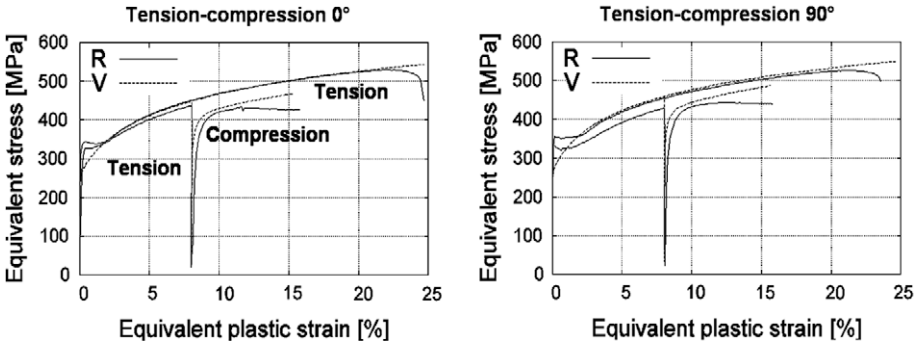

Fig. 14. After direction change from tension into compression the equivalent stress is lower than by forward loading in tensile direction (Bauschinger effect). This effect is observed in real tension–compression tests (R) and is well reproduced from the virtual specimen (V).

ical) material parameters, now tests are carried out with the RVE. With the virtual specimen, there is no limitation to the type and number of experiments for material paramater identification. In this case the Vegter model is chosen.

4.1. Vegter material model

The material model as proposed by Vegter et al. [22] and implemented in PAM-STAMP 2G [15] essentially is a very flexible

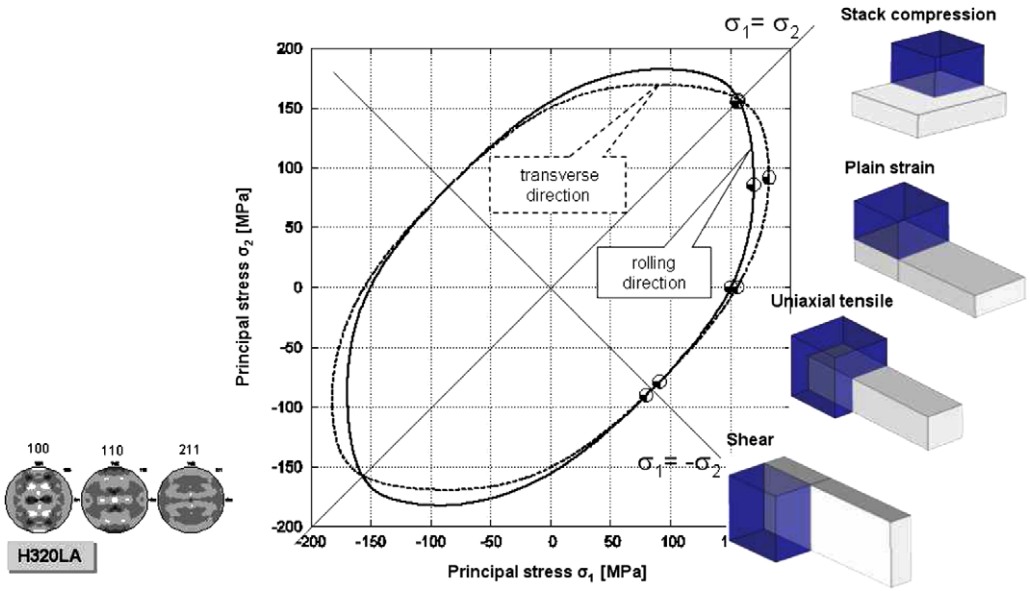

Fig. 15. The Vegter yield locus derived from virtual test data. Single tests are schematically depicted.

description of the yield locus based on interpolation over a high number of tests:

- A stack compression test with measurement of ovalization.
- Three uniaxial tensile tests (0°, 45°, 90°) with lateral strain measurement.
- Three tensile tests with constrained lateral strain (plane strain, 0°, 45°, 90°). Contrary to real tests, the lateral stress can be identified in the virtual tests.

Parameter	Rolling direction		
	0°	45°	90°
σ-uniaxial	1.	1.01	1.029
r-uniaxial	0.624	0.798	0.950
σ-plane strain	1.1	1.14	1.16
α-plane strain	0.5	0.5	0.5
σ-pure shear	0.5615	0.5743	0.603
r-biaxial	0.75	-	-
σ-biaxial	1.004	-	-

Fig. 16. Parameters for the Vegter model (PAM-STAMP 2G [15]) obtained from the virtual tests, H320LA.

- Three shear tests, providing yield locus data in the lower right quadrant for different principal stress directions with respect to rolling direction.

The yield locus is interpolated out of the experimental data by means of cubic Bezier-spline (Fig. 15) The model parameters can be extracted directly from the individual experiments and can be specified subsequently in PAMSTAMP 2G. An explicit fit is only necessary for the hardening parameters (yield curve). The required variables are determined for all experiments at 1% accumulated shear deformation at the slip systems of the virtual specimen. This corresponds to approximately 0.4% plastic strain.

4.2. Springback simulation

The material parameters, obtained from tests with the virtual specimen, are used in springback analysis (Fig. 16).

For a part (Fig. 17) of the car boot (DaimlerChrysler) made of H320LA stamping, trimming and springback are simulated. The differences between real (optically scanned) and simulated geometry are determined. Virtual material testing is expected to provide better agreements between the springback simulation and reality in order to justify the efforts. The simulations using the virtual test data shows greater discrepancies than those using a Hill48 model (Fig. 18) fitted to real tensile test data. If the *r*-values of the virtually fitted Vegter model are replaced by the measured *r*-values, the results are improved. Obviously a significant improvement is not yet achieved. However, the reproduction of tensile strength and

Fig. 17. Stamping part of car boot. Fotos and visualized measured data. After stamping and after trimming.

yield criteria	test data	r0	r45	r90	max. difference [mm]	7.0 5.6 4.2 2.8 1.4 0.0 mm
Hill 48	real correspond to DIN	0.815	1.245	1.087	5.7	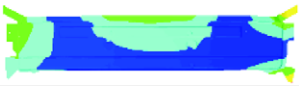
Vegter	virtual, 0.4% plastic strain	0.624	0.798	0.950	6.9	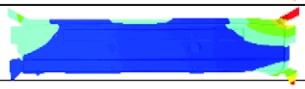
Vegter	virtual and real (r-values)	0.815	1.245	1.087	5.6	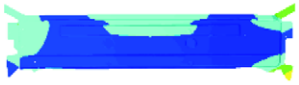

Fig. 18. Shape deviation between measured and simulated geometry for different material models and different types of test data for parameter fitting.

the Bauschinger effect encourage furthermore to improve the virtual specimen.

5. Conclusions

Springback simulation and compensation generate an increasing demand for high precision material models. Microstructural approaches like texture based crystal plasticity still are too expensive in terms of memory and computational power for direct application in industrial sheet metal forming simulations. Therefore, more sophisticated empirical models with various yield loci and hardening laws will continue to emerge. Higher experimental effort for material identification is the price for increasing flexibility and precision of such models. However, microstructural models can be used off-line as virtual specimens to move the effort from the test lab to the computer, thus profiting from continuously decreasing costs per operation.

In this paper a virtual specimen was used to demonstrate the process from model calibration, virtual test program to real part simulation. The particular setting of the virtual model still lacks the important capability to predict the *r*-values correctly. On the other hand, the good prediction of the Bauschinger effect encourages further work. Shortcomings of the presented virtual specimen could be addressed by

- Improved texture sampling for better reproduction of the measured pole figures by discrete grain orientations.
- Account for anisotropy of the grain shape.
- Improved calibration procedure, which should include the latent hardening matrix.

Other extensions could open the model for a wider class of materials, currently being restricted to single phase bcc and fcc metals.

Even with the given restrictions, it was shown that material parameters obtained from texture data and tensile tests using the virtual test program can compete in simulation quality with the full parameter set obtained experimentally.

References

[1] P.J. Armstrong, C.O. Frederick, A Mathematical Representation of the Multiaxial Bauschinger Effect, CEGB Report RD/B/N731, Berkeley Nuclear Laboratories, 1966.
[2] R.J. Asaro, Micromechanics of crystals and polycrystals, in: J.W. Hutchinson, T.Y. Wu (Eds.), Advances in Applied Mechanics, vol. 23, Academic Press, New York, 1983, pp. 1–115.
[3] R.J. Asaro, A. Needleman, Acta Metallica 33 (1985) 923–941.
[4] D. Banabic, H.-J. Bunge, K. Pöhlandt, A.E. Tekkaya, Formability of Metallic Materials, Springer, Berlin, 2000.
[5] F. Barlat, D.J. Lege, J.C. Brem, International Journal of Plasticity 7 (1991) 693–712.
[6] F. Barlat, J. Lian, International Journal of Plasticity 5 (1989) 51–56.
[7] K. Helming, Texturapproximation durch Modellkomponenten (in German). Habilitation Thesis, Technical University Clausthal, Cuvillier Verlag Göttingen, 1998.
[8] K. Helming, R.A. Schwarzer, B. Rauschenbach, S. Geier, B. Leiss, H. Wenk, K. Ullemeier, J. Heinitz, Zeitschrift für Metallkunde 85 (1994) 545–553.
[9] R. Hill, Proceedings of the Royal Society of London A 193 (1948) 281–297.
[10] R. Hill, Journal of the Mechanics and Physics of Solids 38 (1990) 405–417.
[11] S.R. Kalidindi, C.A. Bronkhorst, L.J. Anand, Journal of the Mechanics and Physics of Solids 40 (1992) 537–569.
[12] M. Kraska, Textursimulation bei großen inelastischen Deformationen mit der Technik des repräsentativen Volumenelementes (RVE) (in German), Ph.D. Thesis, Technical University Berlin, Pro Business, Berlin, 1999.
[13] K. Lücke, J. Pospiech, J. Jura, J. Hirsch, Zeitschrift für Metallkunde 77 (1986) 312–321.
[14] K. Lücke, J. Pospiech, K.H. Virnich, J. Jura, Acta Metallica 29 (1981) 167–176.
[15] PAM-STAMP 2G, Version 2004.1 Standard. Stamping Solutions Manual, ESI Group, Paris.
[16] D. Pierce, R.J. Asaro, A. Needleman, Acta Metallica 30 (1982) 1087–1119.
[17] D. Pierce, R.J. Asaro, A. Needleman, Acta Metallica 31 (1983) 1951–1976.
[18] W. Prager, Journal of Applied Mechanics 78 (1956) 493–496.
[19] D. Raabe, F. Roters, International Journal of Plasticity 20 (2004) 339–361.
[20] K. Roll, T. Lemke, K. Wiegand, Possibilities and strategies for simulations and compensation of springback, in: L.M. Smith et al. (Eds.), Proceedings of NUMISHEET 2005, Part A, American Institute of Physics, 2005, pp. 295–302.
[21] C. Teodosiu, Elastic Models of Crystal Defects, Editura Academiei, Bucarest, 1982.
[22] H. Vegter, C. ten Horn, Y. An, E. Atzema, H. Pijlman, A. van den Boogaard, J. Huétink, Characterisation and modelling of the plastic material behaviour and its application in sheet metal forming simulation, in: E. Oñate, D.R.J. Owen (Eds.), Proceedings of COMPLAS VII, CIMNE, Barcelona, 2003.
[23] Z. Zhao, F. Roters, W. Mao, D. Raabe, Advanced Engineering Materials 3 (2001) 984–990.
[24] H. Ziegler, Quarterly of Applied Mathematics 17 (1959) 55–65.